ARTICLE

doi:10.1038/nature10954

Crystal structure of the μ-opioid receptor bound to a morphinan antagonist

Aashish Manglik[1], Andrew C. Kruse[1], Tong Sun Kobilka[1], Foon Sun Thian[1], Jesper M. Mathiesen[1], Roger K. Sunahara[2], Leonardo Pardo[3], William I. Weis[1,4], Brian K. Kobilka[1] & Sébastien Granier[1,5]

Opium is one of the world's oldest drugs, and its derivatives morphine and codeine are among the most used clinical drugs to relieve severe pain. These prototypical opioids produce analgesia as well as many undesirable side effects (sedation, apnoea and dependence) by binding to and activating the G-protein-coupled μ-opioid receptor (μ-OR) in the central nervous system. Here we describe the 2.8 Å crystal structure of the mouse μ-OR in complex with an irreversible morphinan antagonist. Compared to the buried binding pocket observed in most G-protein-coupled receptors published so far, the morphinan ligand binds deeply within a large solvent-exposed pocket. Of particular interest, the μ-OR crystallizes as a two-fold symmetrical dimer through a four-helix bundle motif formed by transmembrane segments 5 and 6. These high-resolution insights into opioid receptor structure will enable the application of structure-based approaches to develop better drugs for the management of pain and addiction.

Opium extracts from the plant *Papaver somniferum* have been used for therapeutic and recreational purposes for thousands of years. Opioid alkaloids and related pharmaceuticals are the most effective analgesics for the treatment of acute and chronic pain. They also represent one of the largest components of the illicit drug market worldwide, generating revenue of approximately $70 billion in 2009, much of which supports crime, wars and terrorism (UNODC World Drug Report 2011). Intravenous use of opioid drugs is a leading cause of death by overdose in Europe and North America, and a major contributing factor to the worldwide AIDS epidemic.

Morphine and codeine are the main active opioid alkaloids in opium. In humans, they act on the central nervous system to produce a wide range of effects including analgesia, euphoria, sedation, respiratory depression and cough suppression, and have peripheral effects such as constipation[1]. Gene disruption studies in mice show that the target for the majority of the effects of opioid alkaloids, whether beneficial or adverse, is the μ-OR[2]. The μ-OR belongs to the γ subfamily of class A G-protein-coupled receptors (GPCRs) with two closely related family members known as the δ- and κ-opioid receptors[3]. The μ-OR constitutes the main opioid target for the management of pain, acute pulmonary oedema, cough, diarrhoea and shivering[1]. However, opioid drugs are highly addictive, with the acetylated form of morphine, heroin, being the best-known example. Because of this, the clinical efficacy of opioid drugs is often limited by the development of tolerance and dependence.

Although both beneficial and adverse effects are attributable to activation of the μ-OR, they seem to be mediated by different downstream signalling and regulatory pathways. The μ-OR couples predominantly to Gi, the inhibitory G protein for adenylyl cyclase. μ-OR signalling through Gi is responsible for its analgesic properties[4]. After activation, the μ-OR undergoes phosphorylation and subsequently couples to arrestins, which have both regulatory and signalling functions[5]. Studies suggest that ligands with the greatest addictive potential, such as morphine, promote interactions with Gi more strongly than they promote interactions with arrestins[6]. These studies suggest that it may be possible to develop safer and more effective therapeutic agents targeting the μ-OR.

To understand better the structural basis for μ-OR function, we performed a crystallographic study of this receptor using the T4 lysozyme (T4L) fusion protein strategy developed previously[7] (Supplementary Fig. 1). Using the *in meso* crystallization method, we obtained crystals and collected diffraction data from 25 crystals of *Mus musculus* μ-OR–T4L protein bound to the irreversible morphinan antagonist β-funaltrexamine (β-FNA). The structure was solved by molecular replacement from a 2.8 Å data set.

Transmembrane architecture

The lattice for the μ-OR receptor shows alternating aqueous and lipidic layers with receptors arranged in parallel dimers tightly associated through transmembrane (TM) helices 5 and 6. More limited parallel interdimeric contacts through TM1, TM2 and helix 8 are observed between adjacent dimers (Supplementary Fig. 2).

As in other GPCRs, the structure of the μ-OR consists of seven TM α-helices that are connected by three extracellular loops (ECL1–3) and three intracellular loops (ICL1–3) (Fig. 1a). TM3 is connected to ECL2 by a conserved disulphide bridge between $C140^{3.25}$ (superscripts indicate Ballesteros–Weinstein numbers[8]) and C217. The morphinan ligand β-FNA (Fig. 1b, c) makes contacts with TM3, TM5, TM6 and TM7 (Fig. 1a), and the electron density observed in the structure confirms previous data identifying the $K233^{5.39}$ side chain as the site of covalent attachment[9] (Fig. 1c and Supplementary Fig. 3).

The intracellular face of the μ-OR closely resembles rhodopsin with respect to the relative positions of TM3, TM5 and TM6 (Supplementary Fig. 4). Nevertheless, like the β_2-adrenergic receptor (β_2-AR), there is no ionic bridge between the DRY sequence in TM3 and the cytoplasmic end of TM6. As with the β_2-AR, $R165^{3.50}$ forms a salt bridge with the adjacent $D164^{3.49}$ of the DRY sequence. $D164^{3.49}$ also engages in a polar interaction with R179 in ICL2, a feature that is similar to an interaction observed between $D130^{3.49}$ and S143 in ICL2

[1]Department of Molecular and Cellular Physiology, Stanford University School of Medicine, Stanford, California 94305, USA. [2]Department of Pharmacology, University of Michigan Medical School, Ann Arbor, Michigan 48109, USA. [3]Laboratori de Medicina Computacional, Unitat de Bioestadística, Universitat Autònoma de Barcelona, Barcelona 08193, Spain. [4]Department of Structural Biology, Stanford University School of Medicine, Stanford, California 94305, USA. [5]CNRS UMR 5203, INSERM U661, and Université Montpellier 1 et 2, Institut de Génomique Fonctionnelle, Montpellier 34094, France.

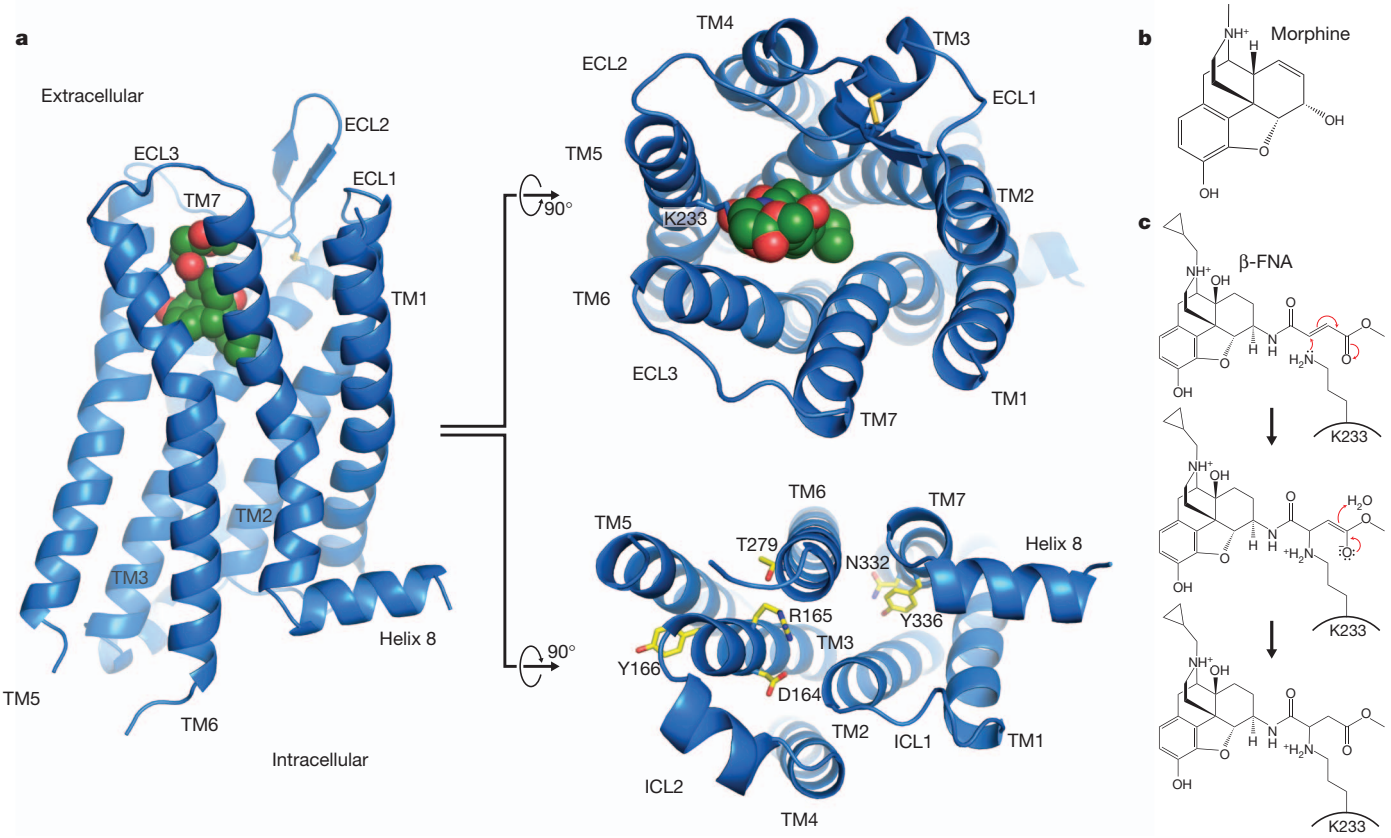

Figure 1 | Overall view of the μ-OR structure. **a**, Views from within the membrane plane (left), extracellular side (top) and intracellular side (bottom) show the typical seven-pass transmembrane GPCR architecture of the μ-OR. The ligand, β-FNA, is shown in green spheres. **b**, The chemical structure of morphine. **c**, The chemical structure of β-FNA and the chemical reaction with the side chain of K233$^{5.39}$ in the receptor are shown. β-FNA is a semisynthetic opioid antagonist derived from morphine, shown in **b**.

of the β_2-AR (Supplementary Fig. 4). In the μ-OR, it has been shown that the mutation of T279$^{6.34}$ to a lysine results in a constitutively active receptor[10]. This may be explained by a polar interaction observed in the crystal structure of the μ-OR between T279$^{6.34}$ and R165$^{3.50}$ (Supplementary Fig. 4). This interaction may stabilize the receptor in an inactive state.

An exposed ligand–binding pocket

In most available GPCR structures, the ligand is partially buried within the helical bundle by more superficial residues in TM segments and ECL2. The most extreme examples are the M2 and M3 muscarinic receptors[11,12], in which the ligand is covered with a layer of tyrosines (Fig. 2). This provides a structural basis for the very slow dissociation

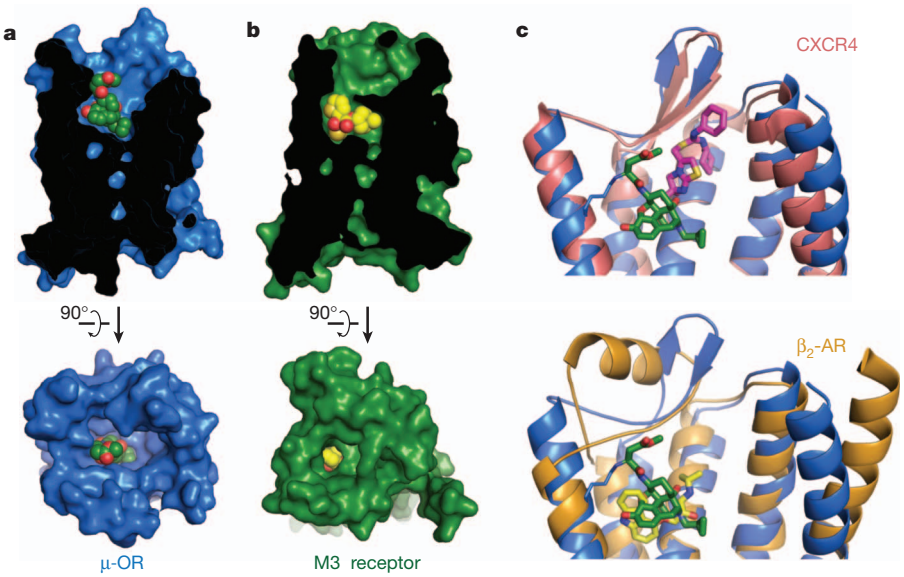

Figure 2 | Comparison of ligand-binding pockets. **a**, **b**, The binding pocket of the μ-OR (**a**) is wide and open above the ligand, in stark contrast to the deeply buried binding pocket of the muscarinic receptors, as exemplified by the M3 receptor (**b**). **c**, Top, the small-molecule antagonist IT1t (magenta) occupies a binding pocket closer to the extracellular surface of CXCR4 than β-FNA in μ-OR. Bottom, β-FNA is positioned more similarly to the distantly related aminergic receptors for the binding site of carazolol (yellow) in the β_2-AR.

kinetics of muscarinic antagonists. For example, the dissociation half-life of the clinically used drug tiotropium at the M3 receptor is 34.7 h and its dissociation constant (K_d) is 40 pM (ref. 13). By contrast, the binding pocket for β-FNA in the μ-OR is largely exposed to the extracellular surface (Fig. 2a). This may explain why extremely potent opioids such as buprenorphine, with an inhibition constant (K_i) of 740 pM, diprenorphine (K_i 72 pM), alvimopan (K_i 350 pM) and etorphine (K_i 230 pM) present rapid dissociation half-lives of 44 min, 36 min, 30 min[14] and less than 1 min (ref. 15), respectively. Therefore, although the affinity of high-affinity opioid ligands is comparable to tiotropium, the dissociation kinetics are considerably different. This feature of opioid ligands may explain why heroin overdoses are rapidly reversible by naloxone[16]. In addition, the extremely high potency and fast kinetics of etorphine agonism and diprenorphine antagonism allows for a system that is capable of rapid anaesthesia and prompt reversal in veterinary use. As a result, etorphine is a preferred anaesthetic (dose in the range of 5–20 $\mu g\,kg^{-1}$) for valuable racehorses and for captive and free-ranging mammals[17].

The μ-OR belongs to a subgroup of peptide GPCRs, and the closest published structure is that of the CXCR4 chemokine receptor[18] (root mean squared deviation (r.m.s.d.) value of 1.35 Å). In the μ-OR the morphinan ligand β-FNA binds much more deeply than the small-molecule CXCR4 antagonist IT1t and occupies a similar position as agonists and antagonists for the β_2-AR (r.m.s.d. value of 1.52 Å) and other monoamine receptors (Fig. 2c).

Binding pocket and opioid specificity

There are 14 residues within 4 Å of β-FNA. Nine of these have more direct interactions with the ligand (Fig. 3a–c), and are conserved in the κ-OR and δ-OR. D147$^{3.32}$ engages in a charge–charge interaction with the amine moiety of the ligand and hydrogen bonds with Y326$^{7.43}$ (both residues are strictly conserved in all the opioid receptor subtypes). Although D147$^{3.32}$ occupies the same position as the counterion in aminergic receptors, a sequence comparison shows that it is not conserved in other peptide receptors. H297$^{6.52}$ interacts with the aromatic ring of the morphinan group, but does not directly hydrogen bond with β-FNA as has been previously suggested[19]. However, the electron density suggests the presence of two water molecules that are well positioned to form a hydrogen-bonding network between H297$^{6.52}$ and the phenolic hydroxyl of the morphinan group (Fig. 3b, c).

A direct comparison with the δ-OR sequence also shows that of the 14 residues within 4 Å of the ligand, 11 are identical between μ-OR and δ-OR. The three differences are at μ-OR positions E229^{ECL2}, K303$^{6.58}$ and W318$^{7.35}$, which are Asp, Trp and Leu in the δ-OR, respectively. The substitution of leucine in δ-OR for W318$^{7.35}$ is highlighted in Fig. 3d. W318$^{7.35}$ was shown to be responsible for the binding selectivity of naltrindole, a δ-OR-selective antagonist and of [D-Pen2,D-Pen5]enkephalin (DPDPE), a δ-OR-selective peptide agonist[20]. In particular, the point mutation W318L markedly increases the affinity of both these ligands at the μ-OR. Positioning naltrindole (represented in Fig. 3d) into the μ-OR-binding pocket by

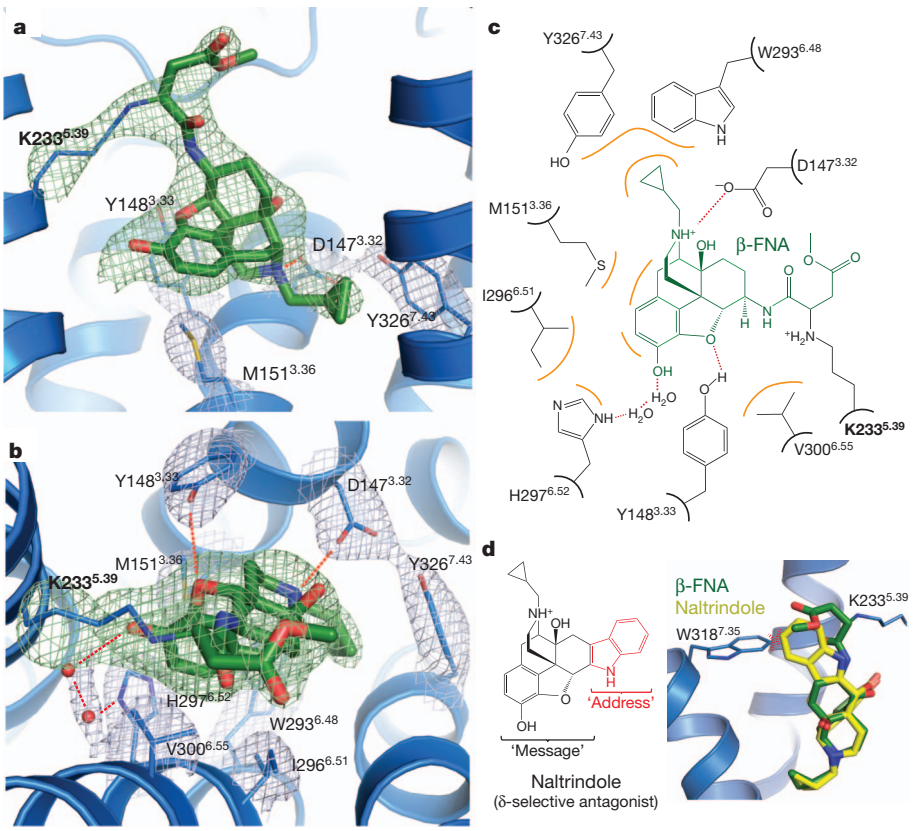

Figure 3 | Structural basis for morphinan ligand binding to the μ-OR. **a**, Side view of the ligand-binding pocket with polar interactions shown. TM6 is excluded from this view. The electron density used to position interacting side chains is shown in light blue coloured mesh depicting the $2F_o - F_c$ electron density contoured at 1.3σ. Green mesh depicts an omit map of β-FNA and K233$^{5.39}$ side-chain atoms contoured at 3.0σ. **b**, Binding pocket viewed from the extracellular surface. Water molecules are shown as red spheres, with the accompanying electron density shown in light blue mesh. **c**, The binding site is diagrammed, showing the chemical structure of β-FNA (green) covalently bound to the receptor through K233$^{5.39}$ (bold). Hydrophobic interactions are shown in orange and polar contacts with red dotted lines. V300$^{6.55}$ and I296$^{6.51}$ form extensive hydrophobic contacts with the back face of the ligand (not shown). Two water molecules are positioned between H297$^{6.52}$ and the phenolic group of β-FNA. **d**, The δ-OR-selective ligand naltrindole includes an indole group that would clash with W318$^{7.35}$ in μ-OR, but not with the leucine found in the equivalent position in δ-OR. The indole has been described as an 'address' to target the ligand to δ-OR, whereas its efficacy ('message') is determined by the morphinan group on the left[40].

superimposition of its morphinan group on that of β-FNA shows that naltrindole would clash with the W318 side chain in μ-OR (Fig. 3d), whereas the leucine in this position of δ-OR would probably accommodate naltrindole without requiring structural rearrangement.

Endomorphins 1 and 2 are small peptides isolated from brain that were shown to have the highest affinity (low nM range) and the highest selectivity profile for the μ-OR receptor[21]. For instance, endomorphin 1 exhibits 4,000- and 15,000-fold selectivity for μ-OR over δ-OR and κ-OR, respectively[21]. Although little is known about the determinants of endomorphin binding, mutagenesis studies suggest that the μ-OR-selective synthetic peptide agonist [D-Ala2,*N*-MePhe4,Gly-ol5] enkephalin (DAMGO) occupies a space that overlaps with the β-FNA-binding pocket but also extends beyond this site[22]. Sites of mutations that impair DAMGO binding include H297$^{6.52}$, positioned near the bottom of the β-FNA pocket, as well as K303$^{6.58}$, W318$^{7.35}$ and H319$^{7.36}$, positioned above the β-FNA-binding pocket (Supplementary Fig. 5). Given the residues involved in DAMGO binding to μ-OR, opioid peptides probably make both polar and non-polar contacts within the μ-OR-binding pocket. This feature of opioid peptide binding is also reflected in the lack of a highly charged surface within the μ-OR-binding pocket compared with that of the CXCR4 receptor[18].

Oligomeric arrangement of μ-OR

The structure of μ-OR shows receptor molecules intimately associated into pairs along the crystallographic two-fold axis through two different interfaces (Fig. 4a, b). The first interface is a more limited parallel association mediated by TM1, TM2 and helix 8, with a buried surface area of 615 Å^2 (Fig. 4d and Supplementary Fig. 6). The second and more prominent interface observed in the μ-OR crystal structure is comprised of TM5 and TM6 (Fig. 4c). In this case, within each μ-OR–μ-OR pair, the buried surface area for a single protomer is 1,492 Å^2. This represents 92% of the total buried surface between μ-OR–T4L molecules, indicating that the comparatively small 114 Å^2 buried surface contributed by T4L is unlikely to drive the contact (Supplementary Fig. 7). This suggests that the pairwise association of receptor monomers may represent a physiological opioid receptor dimer or higher-order oligomer, the existence of which is supported by previous biochemical, pharmacological and cell biological studies[23].

Recent computational and biochemical studies have indicated the potential role of TM4 and TM5 in the interaction between δ-OR receptors[24]. More generally, oligomers have been observed for a large number of GPCRs (recently reviewed in ref. 25). Some of these studies have shown that TM5 and TM6 peptides can disrupt dimers of the β_2-AR and V2 vasopressin receptor[26,27], and recent crosslinking experiments with the M3 muscarinic receptor suggest a direct dimeric contact mediated by TM5 of each monomer[28]. The potential involvement of the alternative TM1–TM2–H8 (where H8 is helix 8) interface in GPCR oligomerization has previously been indicated by several different biochemical studies[25] and, more recently, by the structure of opsin (Protein Data Bank (PDB) accession 3CAP)[29]. In the case of opioid receptors, it has been shown that a μ-OR TM1 domain fused to a polybasic TAT sequence could disrupt the μ-OR–δ-OR interaction in the mouse spinal cord, resulting in an enhancement of morphine analgesia and a reduction in morphine tolerance[30].

The more prominent interface observed in the μ-OR crystal structure is comprised of TM5 and TM6 of each protomer arranged in a four-helix bundle motif (Fig. 5a). This interface is formed by an extensive network of interactions involving 28 residues in TM5 and TM6 (Fig. 5c and Supplementary Fig. 8). These surface packing interactions are highly complementary and are maintained all along the receptor membrane plane from the extracellular to the intracellular side of the μ-OR (Fig. 5c, d). The T279$^{6.34}$ residue described earlier as having a role in maintaining the receptor in an inactive state is also part of the dimer interface, with the methyl of the threonine contacting I256$^{5.62}$ of the adjacent protomer. It is thus tempting to speculate

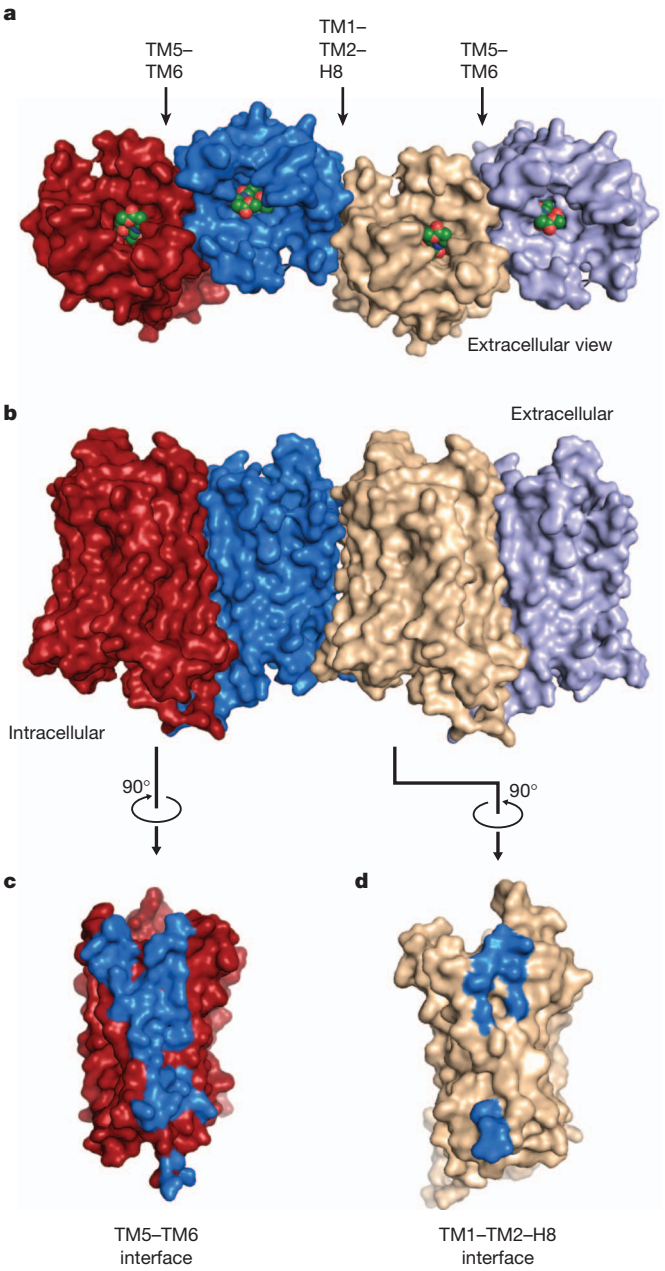

Figure 4 | μ-OR oligomeric arrangement. **a**, **b**, μ-OR crystallized as intimately associated pairs, with two different interfaces as defined in the text. **c**, **d**, The interface defined by TM5 and TM6 (**c**) is much more extensive than for the one defined by TM1–TM2–H8 (**d**).

that dimerization of the μ-OR could have a role in regulating receptor signalling.

The observed dimer is of interest because of existing evidence for both homo- and heterodimers (or oligomers) involving the μ-OR[31]. It has been suggested that opioid agonists such as DAMGO and methadone reduce tolerance to morphine *in vivo* by facilitating morphine-induced endocytosis through μ-OR oligomerization[32,33]. These studies implicate allosteric interactions between a protomer bound to DAMGO or methadone and an adjacent protomer bound to morphine. Co-expressing μ-OR and δ-OR in cells results in pharmacological profiles distinct from either receptor expressed alone[34]. Of interest, morphine is more efficacious in cells expressing both μ-OR and δ-OR in the presence of a δ-OR-selective antagonist, suggesting an allosteric interaction between μ-OR and δ-OR protomers[35]. Hetero-oligomerization between μ-OR and non-opioid receptors has

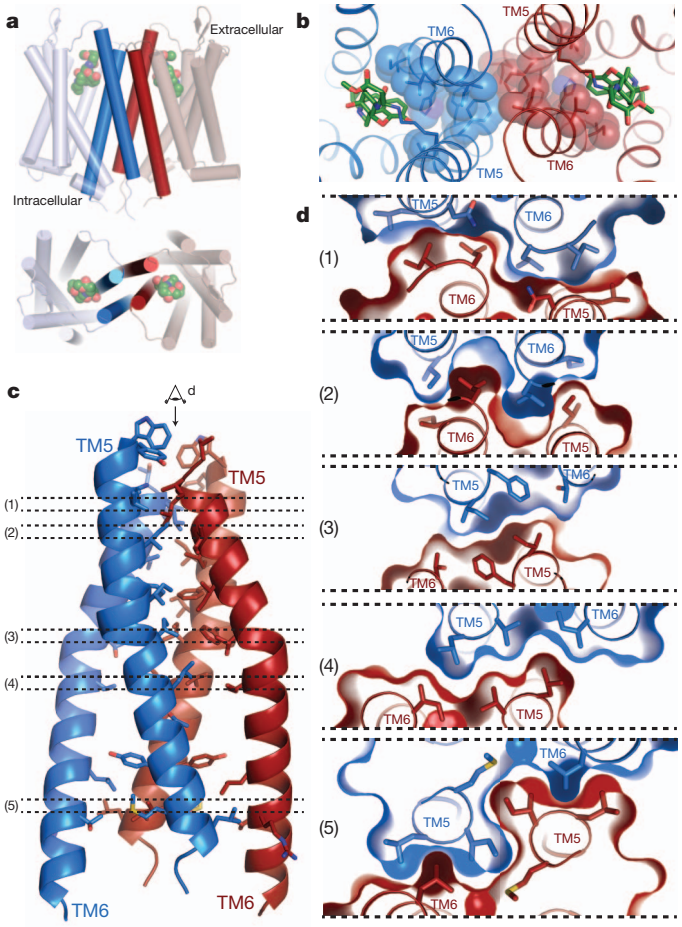

Figure 5 | The four-helix bundle interface. **a**, Schematic showing the four-helix bundle architecture of the TM5–TM6 interface. **b**, Viewed from the extracellular surface, the binding pocket shows tight association between the ligand (green sticks) and residues that are involved directly or indirectly in forming the dimeric interface (blue spheres). **c**, The four-helix bundle is expanded and shown in detail with interacting residues within 4.2 Å shown as sticks. **d**, Tomographic representation along the dimer interface viewed from the extracellular side (as indicated in panel **c**) showing the high surface complementarity within the four-helix bundle interface.

also been reported[23]. For example, the α_{2a} adrenergic receptor was shown to modulate receptor μ-OR structure and signalling[36].

Consistent with a role for oligomerization in μ-OR function, we observed that the amino acids involved in the dimer interface display a high degree of homology with the δ-OR (Supplementary Figs 9 and 10). Replacing the residues of μ-OR with the corresponding residues from δ-OR would not be predicted to interfere with dimer formation (Supplementary Figs 9 and 10). This analysis also suggests that a μ-OR–δ-OR dimer could share the same interface. Interestingly, in the μ-OR TM5–TM6 dimer, the two binding sites are coupled through a network of packing interactions at the dimeric interface (Fig. 5b). This network could provide a structural explanation for the distinct pharmacological profiles obtained for μ-OR heterodimers and for the allosteric effects of one protomer on the pharmacological properties of the other. This dimeric interface thus provides potential insights into the mechanism of allosteric regulation of one GPCR protomer by the other.

Parallel dimers have also been observed in other GPCR crystal structures, most notably in CXCR4–T4L[18]. Interestingly, the CXCR4 dimer is also related by a two-fold rotational symmetry axis with a receptor arrangement similar but not identical to that seen in μ-OR (Supplementary Fig. 8). However, for the five different CXCR4–T4L crystal structures, the largest calculated contact area between the two CXCR4 protomers is smaller (1,077 $Å^2$ for PDB accession 3OE0) than in the μ-OR structure (Supplementary Fig. 7), and it presents a comparatively less extensive network of interactions (Supplementary Fig. 8).

The dimeric arrangement of μ-OR across the TM5–TM6 interface observed in the crystal structure would probably preclude either protomer from coupling to G proteins. This is based on structural changes in TM5 and TM6 observed in the recent crystal structure of the β_2-AR–G_s complex[37]. This is also consistent with the observation that inverse agonists stabilize β_2-AR oligomers, while the G protein G_s reduced the extent of oligomerization[38]. However, we were able to model an active structure of μ-OR in complex with G protein based on the crystal structure of the β_2-AR–G_s complex. Here, we observed that a tetramer formed by the association of two dimers through a TM5–TM6 interface would accommodate two G proteins in interaction with the two distal protomers (Supplementary Fig. 11). This model of an activated μ-OR–G-protein oligomeric complex is highly speculative but is compatible with results from a recent biophysical study suggesting that the G-protein G_i remains associated with a μ-OR tetramer stabilized by the agonist morphine[39].

The μ-OR is perhaps the most economically important GPCR in terms of the combined legal and illicit drug market. Although there are a number of effective drugs targeting the μ-OR on the market, the ideal agonist has yet to be developed. The structure of the μ-OR presented here provides the first high-resolution insight, to our knowledge, into a peptide receptor that can also be activated by small-molecule agonist ligands, some of which are the oldest used drugs in human history. This structure will enable the application of structure-based approaches to complement more conventional drug discovery programs. In addition, it may provide novel insights into the role of oligomerization in GPCR function.

METHODS SUMMARY

The μ-OR–T4L fusion protein was expressed in Sf9 insect cells and purified by nickel affinity chromatography followed by Flag antibody affinity chromatography and size-exclusion chromatography. It was crystallized using the lipidic cubic phase technique, and diffraction data were collected at GM/CA-CAT beamline 23ID-D at the Advanced Photon Source at Argonne National Laboratory. The structure was solved by molecular replacement using merged data from 25 crystals.

Full Methods and any associated references are available in the online version of the paper at www.nature.com/nature.

Received 18 December 2011; accepted 9 February 2012.
Published online 21 March 2012.

1. Katzung, B. G. *Basic and Clinical Pharmacology* 10th edn (LANGE McGraw Hill Medical, 2007).
2. Matthes, H. W. *et al.* Loss of morphine-induced analgesia, reward effect and withdrawal symptoms in mice lacking the μ-opioid-receptor gene. *Nature* **383,** 819–823 (1996).
3. Lord, J. A., Waterfield, A. A., Hughes, J. & Kosterlitz, H. W. Endogenous opioid peptides: multiple agonists and receptors. *Nature* **267,** 495–499 (1977).
4. Raffa, R. B., Martinez, R. P. & Connelly, C. D. G-protein antisense oligodeoxyribonucleotides and μ-opioid supraspinal antinociception. *Eur. J. Pharmacol.* **258,** R5–R7 (1994).
5. Shukla, A. K., Xiao, K. & Lefkowitz, R. J. Emerging paradigms of β-arrestin-dependent seven transmembrane receptor signaling. *Trends Biochem. Sci.* **36,** 457–469 (2011).
6. Molinari, P. *et al.* Morphine-like opiates selectively antagonize receptor-arrestin interactions. *J. Biol. Chem.* **285,** 12522–12535 (2010).
7. Rosenbaum, D. M. *et al.* GPCR engineering yields high-resolution structural insights into β_2-adrenergic receptor function. *Science* **318,** 1266–1273 (2007).
8. Ballesteros, J. A. & Weinstein, H. *Integrated Methods for the Construction of Three Dimensional Models and Computational Probing of Structure Function Relations in G Protein-Coupled Receptors* Vol. 25 366–428 (Academic, 1995).
9. Chen, C. *et al.* Determination of the amino acid residue involved in [^{3}H]β-funaltrexamine covalent binding in the cloned rat μ-opioid receptor. *J. Biol. Chem.* **271,** 21422–21429 (1996).
10. Huang, P. *et al.* Functional role of a conserved motif in TM6 of the rat μ opioid receptor: constitutively active and inactive receptors result from substitutions of Thr6.34(279) with Lys and Asp. *Biochemistry* **40,** 13501–13509 (2001).

11. Haga, K. *et al.* Structure of the human M2 muscarinic acetylcholine receptor bound to an antagonist. *Nature* **482,** 547–551 (2012).
12. Kruse, A. C. *et al.* Structure and dynamics of the M3 muscarinic acetylcholine receptor. *Nature* **482,** 552–556 (2012).
13. Disse, B. *et al.* Ba 679 BR, a novel long-acting anticholinergic bronchodilator. *Life Sci.* **52,** 537–544 (1993).
14. Cassel, J. A., Daubert, J. D. & DeHaven, R. N. [^{3}H]Alvimopan binding to the μ opioid receptor: comparative binding kinetics of opioid antagonists. *Eur. J. Pharmacol.* **520,** 29–36 (2005).
15. Kurowski, M., Rosenbaum, J. S., Perry, D. C. & Sadee, W. [^{3}H]-etorphine and [^{3}H]-diprenorphine receptor binding *in vitro* and *in vivo*: differential effect of Na^+ and guanylyl imidodiphosphate. *Brain Res.* **249,** 345–352 (1982).
16. Sporer, K. A. Acute heroin overdose. *Ann. Intern. Med.* **130,** 584–590 (1999).
17. Alford, B. T., Burkhart, R. L. & Johnson, W. P. Etorphine and diprenorphine as immobilizing and reversing agents in captive and free-ranging mammals. *J. Am. Vet. Med. Assoc.* **164,** 702–705 (1974).
18. Wu, B. *et al.* Structures of the CXCR4 chemokine GPCR with small-molecule and cyclic peptide antagonists. *Science* **330,** 1066–1071 (2010).
19. Mansour, A. *et al.* Key residues defining the μ-opioid receptor binding pocket: a site-directed mutagenesis study. *J. Neurochem.* **68,** 344–353 (1997).
20. Bonner, G., Meng, F. & Akil, H. Selectivity of μ-opioid receptor determined by interfacial residues near third extracellular loop. *Eur. J. Pharmacol.* **403,** 37–44 (2000).
21. Zadina, J. E., Hackler, L., Ge, L. J. & Kastin, A. J. A potent and selective endogenous agonist for the μ-opiate receptor. *Nature* **386,** 499–502 (1997).
22. Seki, T. *et al.* DAMGO recognizes four residues in the third extracellular loop to discriminate between μ- and κ-opioid receptors. *Eur. J. Pharmacol.* **350,** 301–310 (1998).
23. Rozenfeld, R., Gomes, I. & Devi, L. in *The Opiate Receptors* Vol. 23 (ed. Pasternak, G. W.) Ch. 15 407–437 (Humana, 2011).
24. Johnston, J. M. *et al.* Making structural sense of dimerization interfaces of δ opioid receptor homodimers. *Biochemistry* **50,** 1682–1690 (2011).
25. Fanelli, F. & De Benedetti, P. G. Update 1 of: computational modeling approaches to structure-function analysis of G protein-coupled receptors. *Chem. Rev.* **111,** PR438–PR535 (2011).
26. Hebert, T. E. *et al.* A peptide derived from a β_2-adrenergic receptor transmembrane domain inhibits both receptor dimerization and activation. *J. Biol. Chem.* **271,** 16384–16392 (1996).
27. Granier, S. *et al.* A cyclic peptide mimicking the third intracellular loop of the V2 vasopressin receptor inhibits signaling through its interaction with receptor dimer and G protein. *J. Biol. Chem.* **279,** 50904–50914 (2004).
28. Hu, J. *et al.* Structural aspects of M3 muscarinic acetylcholine receptor dimer formation and activation. *FASEB J.* **26,** 604–616 (2011).
29. Park, J. H., Scheerer, P., Hofmann, K. P., Choe, H. W. & Ernst, O. P. Crystal structure of the ligand-free G-protein-coupled receptor opsin. *Nature* **454,** 183–187 (2008).
30. He, S. Q. *et al.* Facilitation of μ-opioid receptor activity by preventing δ-opioid receptor-mediated codegradation. *Neuron* **69,** 120–131 (2011).
31. Jordan, B. A. & Devi, L. A. G-protein-coupled receptor heterodimerization modulates receptor function. *Nature* **399,** 697–700 (1999).
32. He, L., Fong, J., von Zastrow, M. & Whistler, J. L. Regulation of opioid receptor trafficking and morphine tolerance by receptor oligomerization. *Cell* **108,** 271–282 (2002).
33. He, L. & Whistler, J. L. An opiate cocktail that reduces morphine tolerance and dependence. *Curr. Biol.* **15,** 1028–1033 (2005).
34. George, S. R. *et al.* Oligomerization of μ- and δ-opioid receptors. Generation of novel functional properties. *J. Biol. Chem.* **275,** 26128–26135 (2000).
35. Gomes, I., Ijzerman, A. P., Ye, K., Maillet, E. L. & Devi, L. A. G protein-coupled receptor heteromerization: a role in allosteric modulation of ligand binding. *Mol. Pharmacol.* **79,** 1044–1052 (2011).
36. Vilardaga, J. P. *et al.* Conformational cross-talk between α_{2A}-adrenergic and μ-opioid receptors controls cell signaling. *Nature Chem. Biol.* **4,** 126–131 (2008).
37. Rasmussen, S. G. *et al.* Crystal structure of the β_2 adrenergic receptor–G_s protein complex. *Nature* **477,** 549–555 (2011).
38. Fung, J. J. *et al.* Ligand-regulated oligomerization of β_2-adrenoceptors in a model lipid bilayer. *EMBO J.* **28,** 3315–3328 (2009).
39. Golebiewska, U., Johnston, J. M., Devi, L., Filizola, M. & Scarlata, S. Differential response to morphine of the oligomeric state of μ-opioid in the presence of δ-opioid receptors. *Biochemistry* **50,** 2829–2837 (2011).
40. Portoghese, P. S., Sultana, M. & Takemori, A. E. Design of peptidomimetic δ opioid receptor antagonists using the message-address concept. *J. Med. Chem.* **33,** 1714–1720 (1990).

Supplementary Information is linked to the online version of the paper at www.nature.com/nature.

Acknowledgements We acknowledge support from INSERM (S.G.), the Stanford Medical Scientist Training Program (A.M.), the National Science Foundation (A.C.K.), the Lundbeck Foundation (J.M.M.), the National Institutes of Health Grants NS028471 (B.K.K.) and DA031418 (B.K.K. and R.K.S.), and the Mathers Foundation (B.K.K. and W.I.W.).

Author Contributions A.M., A.C.K. and S.G. designed experiments, performed research and analysed data. T.S.K. and F.S.T. expressed and purified receptor. J.M.M. performed preliminary biochemical experiments with wild-type μ-OR. R.K.S. contributed to the effort of μ-OR crystallization and writing of the manuscript. W.I.W. supervised diffraction data analysis and model refinement. L.P. built the tetramer model and helped with the analysis of the dimer interfaces. A.M., A.C.K., S.G. and B.K.K. prepared the manuscript. S.G. and B.K.K. supervised the research.

Author Information Coordinates and structure factors for μ-OR–T4L are deposited in the Protein Data Bank under accession code 4DKL. Reprints and permissions information is available at www.nature.com/reprints. The authors declare no competing financial interests. Readers are welcome to comment on the online version of this article at www.nature.com/nature. Correspondence and requests for materials should be addressed to S.G. (granier@stanford.edu) or B.K.K. (kobilka@stanford.edu).

METHODS

Expression and purification. Previously crystallized GPCRs show little density for the poorly ordered amino- and carboxy-terminal domains. Although these domains are not critical for maintaining high ligand affinity, these flexible regions may inhibit crystallogenesis[7]. We therefore removed these regions in the receptor construct used for crystallography. Specifically, a TEV protease recognition site was introduced after reside G51 in the amino terminus and the C terminus was truncated after Q360. The short third intracellular loop of μ-OR, consisting of residues 264–269, was replaced with T4L residues 2–161 in a manner described previously[7]. To facilitate receptor purification, a Flag M1 tag was added to the N terminus and an octa-histidine tag was appended to the C terminus. Finally, a proline residue was introduced N-terminal to the octahistidine tag to allow efficient removal of C-terminal histidines by carboxypeptidase A. For these studies, we used the *M. musculus* μ-OR sequence because it is expressed at higher levels. The mouse and human μ-OR share 94% sequence identity and there are only four residues in the resolved part of the structure that differ between the mouse and human μ-OR. These include residues 66, 137, 187 and 306, which are all in the extracellular or intracellular loops of μ-OR and do not make contacts in the ligand-binding pocket. The final crystallization construct (μ-OR–T4L) is shown in a representative snake diagram in Supplementary Fig. 1a.

We compared the pharmacological properties of μ-OR–T4L to those of the wild-type receptor (Supplementary Fig. 1b). Both constructs showed identical affinity for the radiolabelled antagonist [^{3}H]-diprenorphine ([^{3}H]DPN).

The μ-OR–T4L construct was expressed in Sf9 cells using the baculovirus system. Culture media was supplemented with 10 μM naloxone to stabilize the receptor during expression. Cells were infected at a density of 4×10^6 cells per ml and culture flasks were shaken at 27 °C for 48 h. After harvesting, cells were lysed by osmotic shock in a buffer comprised of 10 mM Tris-HCl pH 7.5, 1 mM EDTA, 100 μM TCEP, 1 μM naloxone and 2 mg ml^{-1} iodoacetamide to block reactive cysteines. Extraction of μ-OR–T4L from Sf9 membranes was done with a Dounce homogenizer in a solubilization buffer comprised of 0.5% dodecyl maltoside (DDM), 0.3% 3-[(3-Cholamidopropyl) dimethylammonio]-1-propanesulphonate (CHAPS), 0.03% cholesterol hemisuccinate (CHS), 20 mM HEPES pH 7.5, 0.5 M NaCl, 30% v/v glycerol, 2 mg ml^{-1} iodoacetamide, 100 μM TCEP and 1 μM naloxone. After centrifugation, nickel-NTA agarose was added to the supernatant, stirred for 2 h, and then washed in batch with 100*g* spins for 5 min each with a washing buffer of 0.1% DDM, 0.03% CHAPS, 0.01% CHS, 20 mM HEPES pH 7.5 and 0.5 M NaCl. The resin was poured into a glass column and bound receptor was eluted in washing buffer supplemented with 300 mM imidazole.

We used anti-Flag M1 affinity resin to purify μ-OR–T4L further and to exchange the ligand with the covalent antagonist β-FNA. Nickel-resin eluate was loaded onto anti-Flag M1 resin and washed extensively in the presence of 10 μM β-FNA. The detergent DDM was then gradually exchanged over 1 h into a buffer with 0.01% lauryl maltose neopentyl glycol (MNG) and the NaCl concentration was lowered to 100 mM. Receptor was eluted from the anti-Flag M1 affinity resin with 0.2 mg ml^{-1} Flag peptide and 5 mM EDTA in the presence of 1 μM β-FNA. To remove the N terminus of μ-OR–T4L, TEV protease was added at 1:3 w/w (TEV:μ-OR–T4L) and incubated at room temperature (23 °C) for 1 h. Receptor was then treated with carboxypeptidase A (1:100 w/w) and incubated overnight at 4 °C to remove the octa-histidine tag. The final purification step separated TEV and carboxypeptidase A from receptor by size exclusion chromatography on a Sephadex S200 column (GE Healthcare) in a buffer of 0.01% MNG, 0.001% CHS, 100 mM NaCl, 20 mM HEPES pH 7.5 and 1 μM β-FNA. After size exclusion, β-FNA was added to a final concentration of 10 μM. The resulting receptor preparation was pure and monodisperse (Supplementary Fig. 12).

Crystallization and data collection. Purified μ-OR–T4L receptor was concentrated to 30 mg ml^{-1} using a Vivaspin sample concentrator with a 50 kDa molecular weight cut-off (GE Healthcare) and crystallization was performed using the *in meso* method[41]. Concentrated μ-OR–T4L was reconstituted into 10:1 monoolein:cholesterol (Sigma) in a ratio of 1:1.5 parts by weight receptor:lipid mixture. Reconstitution was done by the two-syringe method[41]. The resulting mesophase was dispensed onto glass plates in 80-nl drops and overlaid with 700 nl precipitant solution by a Gryphon LCP robot (Art Robbins Instruments). Crystals grew in precipitant solution consisting of 30–38% PEG 400, 100 mM HEPES pH 7.0, 7.5% DMSO and 300 mM lithium sulphate. Crystals were observed after 24 h and grew to full size after 5 days. Typical crystals before harvesting are shown in Supplementary Fig. 2.

Diffraction data were collected at Advanced Photon Source GM/CA-CAT beamline 23ID-D using a beam size of 10 μm. Owing to radiation damage, the diffraction quality decayed during exposure. Wedges of 10–20 degrees were collected and merged from 25 crystals using HKL2000[42]. Diffraction quality ranged from 2.4–3.5 Å in most cases. The structure of the μ-OR was solved by molecular replacement in Phaser[43] using the CXCR4 receptor as a search model. We improved the initial model by iteratively building regions of the receptor in Coot[44] and refining in Phenix[45]. We used translation libration screw-motion (TLS) refinement with groups generated within Phenix. Electron density suggested the presence of a cholesterol molecule and a monoolein lipid within the lipidic layer. These were subsequently incorporated into the model. To assess the overall quality of the final structure, we used MolProbity[46]. The resulting statistics for data collection and refinement are shown in Supplementary Table 1. Figures were prepared in PyMOL[47].

Saturation binding experiments. Membrane homogenates were prepared from Sf9 cells expressing either wild-type μ-OR or μ-OR–T4L. Membranes containing μ-OR or μ-OR–T4L were incubated with the opioid antagonist, [^{3}H]DPN for 1 h at 22 °C in 0.5 ml of binding buffer containing 75 mM Tris-HCl pH 7.4, 1 mM EDTA, 5 mM $MgCl_2$, 100 mM NaCl. To determine the affinity for diprenorphine, we used [^{3}H]DPN concentrations ranging from 0.1 to 13.5 nM. High concentrations of un-labelled naloxone (1 μM) were used to determine non-specific binding. To separate unbound [^{3}H]-ligand, binding reactions were rapidly filtered over GF/C Brandel filters. The filters were then washed three times with 5 ml ice-cold binding buffer. Radioactivity was assayed by liquid scintillation counting. The resulting data were analysed using Prism 5.0 (GraphPad Software). [^{3}H]DPN (specific activity: 55.0 Ci mmol^{-1}) was obtained from PerkinElmer Life Sciences.

41. Caffrey, M. & Cherezov, V. Crystallizing membrane proteins using lipidic mesophases. *Nature Protocols* **4,** 706–731 (2009).
42. Otwinowski, Z. & Minor, W. Processing of X-ray diffraction data collected in oscillation mode. *Methods Enzymol.* **276,** 307–326 (1997).
43. McCoy, A. J. *et al.* Phaser crystallographic software. *J. Appl. Cryst.* **40,** 658–674 (2007).
44. Emsley, P. & Cowtan, K. Coot: model-building tools for molecular graphics. *Acta Crystallogr. D* **60,** 2126–2132 (2004).
45. Afonine, P. V., Grosse-Kunstleve, R. W. & Adams, P. D. A robust bulk-solvent correction and anisotropic scaling procedure. *Acta Crystallogr. D* **61,** 850–855 (2005).
46. Chen, V. B. *et al.* MolProbity: all-atom structure validation for macromolecular crystallography. *Acta Crystallogr. D* **66,** 12–21 (2010).
47. Schrodinger, L. The PyMOL Molecular Graphics System v.1.3r1. (2010).